
PHOTON-PAIR GENERATION IN A HETEROGENEOUS SILICON PHOTONIC CHIP

Mingwei Jin^{1,2,†}, Neil MacFarlane^{3,†}, Zhaohui Ma^{1,2}, Yongmeng Sua^{1,2}
 Mark A. Foster³, Yuping Huang^{1,2}, Amy C. Foster³

†. Equally contributing authors

1. Department of Physics, Stevens Institute of Technology, Hoboken, NJ, 07030, USA

2. Center for Quantum Science and Engineering, Stevens Institute of Technology, Hoboken, NJ, USA

3. Department of Electrical and Computer Engineering, Johns Hopkins University, 3400 North Charles Street, Baltimore MD, 21218, USA

August 31, 2022

ABSTRACT

Integrated Silicon photonics has played an important role in advancing the applications of quantum information and quantum science. However, due to different material properties, it is challenging to integrate all components with excellent performance based on homogeneous material. Here, by combining high nonlinearity and low losses in a heterogeneous silicon platform, we efficiently generate high-quality photon pairs through spontaneous four-wave mixing in hydrogenated amorphous silicon waveguide and route them off-chip through low loss silicon nitride waveguide. A record high coincidence- to- accidental rate value of $1632.6 (\pm 260.4)$ is achieved in this heterogeneous design with a photon pair generation rate of 1.94 MHz. We also showcase a wide range of multi-channel photon sources with coincidence- to- accidental rate consistently at 200. Lastly, we measure heralded single-photons with a lowest $g_H^{(2)}(0)$ of 0.1085 ± 0.0014 . Our results demonstrate the heterogeneous silicon platform as an ideal platform for efficient generation of photon pairs and routing them off-chip with low losses. It also paves a way for the future hybrid photonic integrated circuit by collecting distinct features from different materials.

1 Introduction

Integrated photonics has emerged as a key technology in various applications such as data centers, telecommunication, photonic computing, and quantum computing. These applications require numerous integrated components including low-loss waveguide routing, laser sources, photodetectors, modulators, single photon and photon pair sources. However, due to distinct properties of different materials, it becomes necessary to incorporate various materials in heterogeneous platforms to incorporate different components onto a single platform Davanco et al. [2017], Schnauber et al. [2019], Moody et al. [2022].

Among those photonic components, correlated photon-pair sources are of great interest due to their applications in quantum computing, quantum teleportation, quantum information processing, quantum sensing, quantum cryptography and others O’Brien [2007], Bouwmeester et al. [1997], Kimble [2008], Degen et al. [2017], Gisin et al. [2002], O’Brien et al. [2009]. A photon pair source with a broad and switchable bandwidth is essential for applications such as quantum frequency multiplexing and quantum memory Lavoie et al. [2013], Sinclair et al. [2014]. Over the past decade, there has been tremendous progress with chip-integrated photon pair sources by spontaneous four-wave mixing (SFWM) and spontaneous parametric down-conversion (SPDC), such as those in crystalline silicon (c-Si) Kues et al. [2017], Lu et al. [2016], silicon nitride (Si_3N_4) Zhang et al. [2016], hydrogenated amorphous Silicon (a-Si:H) Wang et al. [2014], Hemsley et al. [2016], gallium phosphide (GaP) Logan et al. [2018], gallium arsenide (GaAs) Chang et al. [2019], and lithium niobate (LiNbO_3) Ma et al. [2020]. Among these platforms, a-Si:H has achieved particular attention as

a photonic platform due to its ultra-high Kerr nonlinearity ($n_2 = 7.43 \pm 0.87 \times 10^{-13} \text{ cm}^2/\text{W}$) comparing to other silicon-based material platforms Wang and Foster [2012]. With such a high Kerr coefficient, efficient SFWM can be achieved with only millimeters of waveguide propagation. Contending with crystalline Silicon (c-Si), a-Si:H can be easily deposited at a lower temperature and thus incorporated in massive chip manufacturing processes Hemsley et al. [2016].

Despite the excellent Kerr nonlinearity of a-Si:H, the lowest reported a-Si:H linear propagation losses are about an order of magnitude higher than Si_3N_4 Oo et al. [2019]. In quantum application, Even though the high nonlinearity of a-Si:H plays a key role in efficiently generating photon pairs, the high propagation loss of a-Si:H waveguide results in many of the photon pairs being lost on chip before off-chip detection. This dramatically reduces the coincidence- to- accidental rate that can be observed and severely limits its quantum applications.

In our previous work, to mitigate higher propagation losses in a-Si:H waveguides, Si_3N_4 waveguides are used for on/off-chip coupling, and vertical coupling between a-Si:H and Si_3N_4 occurs on-chip MacFarlane et al. [2019]. With a careful design of vertical coupler, the coupling loss is optimized around 0.5 dB per transition. The replacement of the a-Si:H with a Si_3N_4 waveguide for on-off chip coupling dramatically reduces fiber-to-fiber loss. This reduces the required pump power especially for photon pair generation and broadens the applications of such a platform to other quantum technologies.

In this paper, leveraging the low loss and high nonlinearity of the heterogeneous platform, we further explore the quantum performance of a-Si:H/ SiN_x waveguides. We experimentally demonstrate the photon pair generation with the highest coincidence- to- accidental rate (CAR) of $1632.6 (\pm 260.4)$ in non-resonant a-Si:H waveguides, showing significant improvement comparing to the previous state of the art value in non-resonant a-Si:H waveguide Wang et al. [2014]. The pure photon pairs are measured at multiple channels with a detuning bandwidth of 6 nm and CAR value consistently at 200. In addition, with the same chip, we perform heralded generation of single photons. The auto-correlation is measurement as low as 0.0126 ± 0.005 . Our work combines the high nonlinearity of a-Si:H and the low propagation loss of Si_3N_4 . Our results demonstrate the benefits of a heterogeneous silicon platform for quantum applications by utilizing both low transmission loss and highly nonlinearity. With low-loss inter-layer coupler, such heterogeneous silicon platform also paves the way for integrating even more layers and materials to achieve high-quality components for various applications in quantum applications.

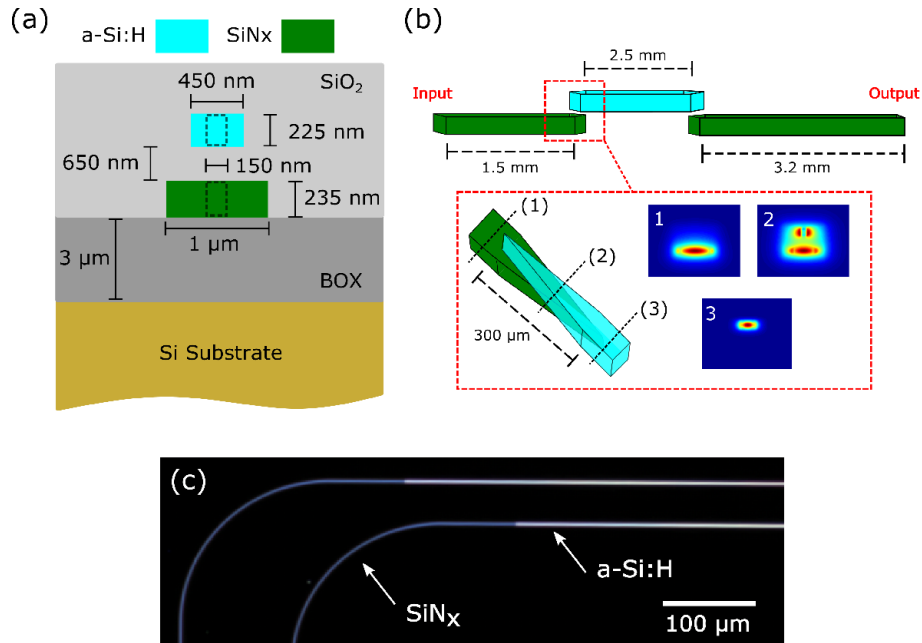


Figure 1: (a) Cross-section of multi-layer platform. (b) Side view of device showing propagation lengths in SiN_x (green) and a-Si:H (blue) waveguides. (Inset - Top-down view of interlayer coupler with electric field profiles at three locations along the interlayer coupler). (c) Dark-field microscope image of SiN_x /a-Si:H waveguides and interlayer coupling region.

2 Experimental Results

The multi-layer architecture is shown in Figure 1 (a-c). The device fabrication starts with a 100-mm silicon wafer with a 3- μm thick layer of thermal oxide on its surface. 240 nm of SiN_x is deposited using low-pressure chemical vapor deposition (LPCVD). The recipe parameters consisted of a deposition rate of 4-nm/min, a temperature of 775 $^\circ\text{C}$, 1000-MPa tensile stress, and 250 mTorr chamber pressure. Platinum marks for alignment between layers were patterned using electron beam lift-off lithography. Waveguides in the SiN_x layer were patterned and etched by e-beam lithography and reactive ion etching respectively. The Silicon dioxide (SiO_2) cladding was then deposited with plasma-enhanced chemical vapor deposition (PECVD). Planarization of the SiO_2 surface was performed using chemical mechanical polishing. 225-nm of a-Si:H was then deposited by PECVD. The a-Si:H layer was deposited using recipe parameters of a temperature of 300 $^\circ\text{C}$, a RF power of 15-W, 1000-SCCM of 5% silane/helium gas flow, and 1800 mTorr chamber pressure. With the lower a-Si:H deposition temperature we are able to deposit it directly on top of the SiN_x waveguides without damaging them. Finally, a-Si:H waveguides are patterned and etched using e-beam lithography and reactive ion etching. The a-Si:H waveguides are clad with PECVD (SiO_2) and individual chips are diced out of the wafer. Figure 1 (b) shows the geometry of the interlayer coupler. The optical modes at different coupler sections are simulated as figure 1 (b). Figure 1 (c) shows a dark-field microscope image of SiN_x and a-Si:H waveguides and the interlayer coupling region.

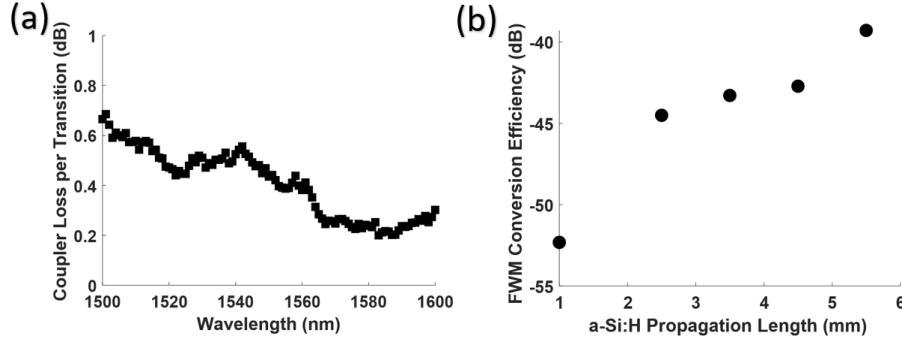


Figure 2: (a) Interlayer coupler loss per wavelength. (b) FWM conversion efficiency for different propagation lengths of a-Si:H waveguides. (originally published in MacFarlane et al. [2022])

To characterize the Kerr coefficient of a-Si:H waveguides, we first perform classic degenerate FWM in our multi-layer devices. Light is coupled on/off chip via inverse taper couplers in the SiN_x layer as shown in Figure 1 (b). We couple on/off the chip using tapered lensed fibers with mode-field diameters of 2.5 μm . The SiN_x layer offers improved fiber-to-chip coupling efficiency from better mode-matching with the lensed fiber compared to the a-Si:H waveguides. Once on-chip, the light propagates for 1.5 mm in the SiN_x layer and is then coupled to the a-Si:H layer via evanescent inverse taper couplers and propagates for varying a-Si:H lengths between 1 mm and 5.5 mm. The signal is then coupled back to the SiN_x layer, where it propagates for another 3.2 mm and is finally output via the SiN_x layer and coupled to a tapered lensed fiber. The on-chip interlayer coupling insertion loss is measured to be less than 1 dB per transition over a 100 nm bandwidth, while the propagation losses in the SiN_x and a-Si:H waveguides are 0.5 dB/cm and 4 dB/cm, respectively. The insertion losses as a function of wavelength are shown in Figure 2 (a). We measure the four-wave mixing conversion efficiency (CE), defined as the ratio of the output idler power to the input signal power, using multiple devices with varying propagation lengths in the a-Si:H layer. The measured conversion efficiency values as a function of a-Si:H propagation length are shown in Figure 2 (b). These results equate to a Kerr coefficient of $\sim 5 \times 10^{-13} \text{ cm}^2/\text{W}$, which is comparable to the state-of-the-art value ($7.43 \times 10^{-13} \text{ cm}^2/\text{W}$) Wang and Foster [2012].

The photon pairs are then generated through SFWM in the a-Si:H waveguides. In figure 3 (a), a 50MHz mode lock laser(Calmar Mendocino) is connected with a variable attenuator and four cascaded dense wavelength-division multiplexing (DWDM) filters at 1552.5 nm to accurately control pump power and suppress photons beyond pump wavelength, respectively. We couple to the TE waveguide mode for optimum SFWM efficiency and broad bandwidth by carefully tuning a fiber polarization controller (FPC) and couple to the SiN_x inverse taper coupler through a lensed fiber. After propagating in the SiN_x waveguide, light is coupled through an interlayer coupler to a 2.5 mm long a-Si:H waveguide where the photon-pair is generated. The generated photon-pair is coupled back to a low-loss SiN_x waveguide and collected by a lensed fiber at the output. The total on-off chip loss is 9 dB. The remaining pump photons are immediately rejected by two cascaded DWDM filters with labelled 60 dB extinction. Two DWDM filters at 1545.3 nm collect Stokes photons and reject all other wavelengths. The anti-Stokes photon at 1559.7nm is collected by two other DWDMs. The bandwidth for the DWDM filters are aligned to be 200 GHz. The total losses by the output DWDM sets are 1.9 dB and 2.2 dB at Stokes and anti-Stokes channels, respectively. To ensure maximum detection efficiency, two

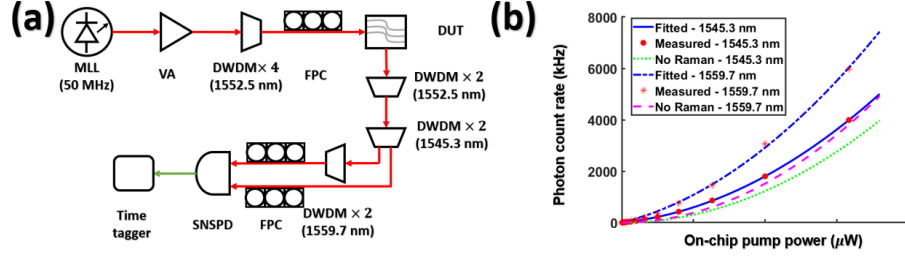


Figure 3: (a) Experimental setup. MLL: mode locked laser. VA: variable attenuator. DWDM: dense wavelength-division multiplexer. FPC: fiber polarization controller. DUT: device under test. SNSPDs: superconducting nanowire single photon detectors. (b) Single photon counts of Stokes and anti-Stokes channels versus the on-chip pump power. ((b) originally published in MacFarlane et al. [2022])

FPCs are placed before entering superconducting nanowire single photon detectors (4 channels SNSPDs, ID281, ID Quantique). The SNSPDs have dark-count rate of 50-100 Hz and detection efficiency of 85%. The detected signals are lastly resolved by a time-tagging unit (Swabian Instruments) for photon counting and correlated detection.

The stimulated Raman scattering (SRS) noise is first characterized by measuring the power-dependent single photon counts. In the waveguide, the SRS generated photons are linearly proportional to the on-chip pump power P_{in} while the SFWM generated photons are proportional to P_{in}^2 . Thus, SRS noise can be abstracted at Stokes and anti-Stokes channels by fitting the curves as shown in figure 3 (b).

Figure 4 (a) shows the coincidence-to-accidental ratios (CAR) versus on-chip pump power. The dark count has been subtracted from coincidence and accidental counts to eliminate dark-count noise, which may significantly decrease CAR in the low count rate regime. The highest CAR is achieved at 1632.6 (± 260.4) with average on-chip pump power of about -30.5 dBm. The corresponding photon pair generation rate (PGR) is measured and estimated to be 1.94 MHz. The CAR then drops to 1335.3 (± 240.9) when further lowering on-chip pump power. This occurs because the background noise contributes more to the result when the count rates of Stokes and anti-Stokes photons are closer to the dark-count level. Figure 4 (b) plots coincidence measurement at the highest measured CAR. The coincidences are counted using the full width at half maximum (FWHM) of the pulse which is depicted in the upper inset. The lower inset shows the accidental counts and background noise. Figure 4(c) plots PGR at low on-chip pump power regime. The error bars are within the dotted areas. The coincidence rate is measured on the same run of CAR measurement. The PGR is then estimated as $N_1 N_2 / N_{12}$, where N_1 , N_2 and N_{12} denotes the detection rate of signal, idler and two-photon coincidences.

Figure 4 (d) depicts CAR measurement for multi-channel photon-pairs. To measure the CAR at different wavelength channels, instead of using DWDMs to select the signals and idlers, the photon pairs are filtered using a programmable waveshaper. The waveshaper introduces an additional 5 dB loss, which increases the required pump power. With on-chip pump power at -20.5 dBm, the CAR remains about 200 for the wavelength detuning from 4.2 nm to 10.2 nm. This showcases a wide bandwidth for photon-pair generation that can be dispersion engineered into these devices.

The heralded single-photon generation and the auto-correlation function ($g_H^{(2)}(\tau)$) are important for ensuring the purity of photon pair source. As is shown in Figure 5 (a), to measure the heralded single-photon generation, the idler is separated by a 50/50 splitter into two as idler I and idler II. Then together with signal, they are all sent into SNSPD to measure double coincidences between signal and Idler I (N_{12}), Idler II (N_{13}) and triple coincidences N_{123} . The auto-correlation function of $g_H^{(2)}(\tau)$ is then calculated by $N_{123} N_1 / N_{12} N_{13}$, where N_1 denotes signal detection rate. Using the programmable time-tagging unit, the coincidence rates at different time delays can be measured during the same experimental run. This is enabled by duplicating the detected physical photon channel to multiple virtual channels with different time delays and thus all corresponding coincidences are measured at once. This method largely simplifies the experiment and reduces noise and instabilities induced by different experimental runs. Figure 5 (b) plots the auto-correlation function with zero time delay, which is normalized to the averaged $g_H^{(2)}(\tau)$ at other 20 ns-delays (corresponding to the 50 MHz repetition rate of our MLL). The lowest $g_H^{(2)}(0)$ is measured to be 0.0126 ± 0.005 at an on-chip power of -22.5 dBm and N_1 of 18 kHz. It increases to 0.1085 ± 0.0014 at on-chip power of -16.3 dBm and N_1 of 310 kHz. This $g_H^{(2)}(\tau)$ measurement indicates our heterogeneous chip is a versatile single and paired photon sources for a variety of quantum optical information technologies.

Table 1 shows the state of the art of photon pair generation through $\chi^{(3)}$ process. Comparing with the previous result in a pure a-Si:H platform, our device has exhibited 4 times higher CAR and 30 times higher PGR due to much lower

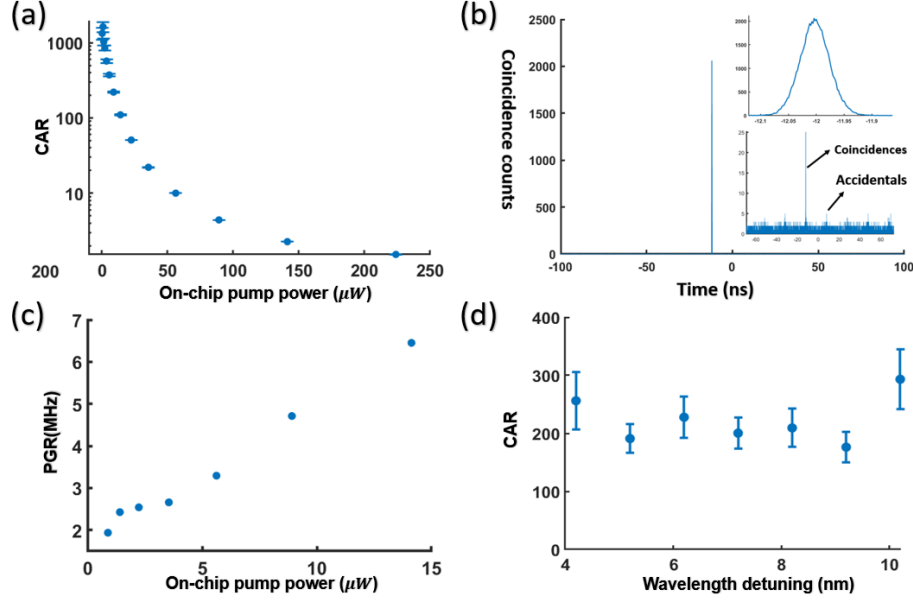


Figure 4: (a) CAR versus the on-chip pump power. (b) Coincidences measurement at CAR of $1632.6 (\pm 260.4)$. The upper inset shows the coincidences at zero time delay. The lower inset shows the background noise and accidental at non-zero time delays. (c) Photon pair generation rate (PGR) at low power regime. (d) CAR for different wavelength channels. ((a) and (d) originally published in MacFarlane et al. [2022])

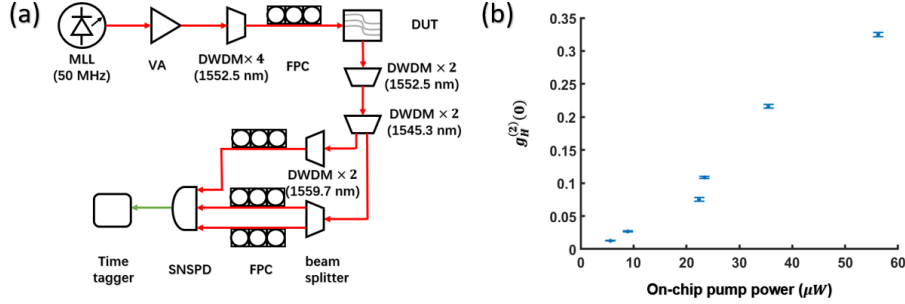


Figure 5: (a) Experimental setup for heralded single-photon generation. (b) normalized auto-correlation function with zero time delay $g_H^{(2)}(0)$ at different on-chip pump powers

propagation/coupling loss through the waveguide. With the CAR higher than 1000, our work features a high PGR of 1.94 MHz. This shows that our device can massively produce high quality photon pairs. Leveraging high the nonlinearity of a-Si:H waveguide, the photon pairs can be produced efficiently through our non-resonant waveguide without the nonlinearity enhancement by microring. This allows more freedom of wavelength selection and avoid the instabilities of resonance shifting due to the thermo-optic effect or nonlinear phase modulation from a strong pump. Our showcase this heterogeneous a-Si:H/ Si_3N_4 platform as an excellent and stable platform for photon pair and single photon generation.

3 Conclusion

In this paper, utilizing the high nonlinearity of a-Si:H for efficient photon pair generation and low loss of SiN_x for the routing of photon pairs, we have experimentally demonstrated photon-pair generation with a record high CAR of 1632.6 (± 260.4) for non-resonant a-Si:H waveguides, which shows 4-times improvement compared to the previous single-layer a-Si:H platform Wang et al. [2014]. We also demonstrate multi-channel photon-pair sources with a CAR of around 200 across 10-nm bandwidth. Additionally, we have measured the heralded single-photon generation and demonstrated low correlation function of $g_H^{(2)}(0)$ at 0.0125 ± 0.005 . Our results show that with the increased coupling efficiency and low propagation losses of the SiN_x waveguide, higher photon detection rate can be observed with much lower on-chip pump power. This enables us to achieve a high CAR and high photon pair generation rate. The multi-material deposition and low-loss interlayer couplers has enabled a way to combine different materials' features onto the single platform

Table 1: The state of the art of photon pair generation through $\chi^{(3)}$ process

Reference	Material	On-chip pump power	CAR	PGR	$g_H^{(2)}$
K. Wang(2014)Wang et al. [2014]	a-Si:H	$18 \mu W$	399	65 kHz	...
This work	a-Si:H/Si ₃ N ₄	$0.9 \mu W$	1632.6	1.94 MHz	...
This work	a-Si:H/Si ₃ N ₄	$5.6 \mu W$	373.3	3.29 MHz	0.0126
W. Jiang(2015)Jiang et al. [2015]	c-Si disk	$79 \mu W$	274	855 kHz	...
X. Lu(2016)Lu et al. [2016]	c-Si disk	$12 \mu W$	2610	1.2 kHz	0.003
C. Ma(2017) Ma et al. [2017]	c-Si ring	$7.4 \mu W$	12105	16 kHz	0.005
C. Ma(2017) Ma et al. [2017]	c-Si ring	$59 \mu W$	532	1.1 MHz	0.005
X. Lu(2019) Lu et al. [2019]	Si ₃ N ₄ ring	$46 \mu W$	2280	4.8 kHz	...
T. Steiner(2021)Steiner et al. [2021]	AlGaAsOI ring	$3.4 \mu W$	4389	230KHz	0.004

and flexibly transfer photons and optical signals between different layers and materials with low transition loss. This solution offers the possibility for the future PICs to integrate components from other material platforms and further miniaturize the experimental setups used in this work, for example χ^2 nonlinearity and electro-optic modulation from lithium niobate, laser source from III-V materials, and photodetectors from germanium Chen et al. [2019], Wang et al. [2018], Jin et al. [2021], Keyvaninia et al. [2013], Guo et al. [2019], Michel et al. [2010], Marris-Morini et al. [2018].

4 Acknowledgement

This research was supported in part by National Science Foundation (#1641094).

References

- Dik Bouwmeester, Jian-Wei Pan, Klaus Mattle, Manfred Eibl, Harald Weinfurter, and Anton Zeilinger. Experimental quantum teleportation. *Nature*, 390(6660):575–579, Dec 1997. ISSN 1476-4687. doi:10.1038/37539. URL <https://doi.org/10.1038/37539>.
- Lin Chang, Andreas Boes, Paolo Pintus, Jon D. Peters, MJ Kennedy, Xiao-Wen Guo, Nicolas Volet, Su-Peng Yu, Scott B. Papp, and John E. Bowers. Strong frequency conversion in heterogeneously integrated gas resonators. *APL Photonics*, 4(3):036103, 2019. doi:10.1063/1.5065533. URL <https://doi.org/10.1063/1.5065533>.
- Jia-Yang Chen, Zhao-Hui Ma, Yong Meng Sua, Zhan Li, Chao Tang, and Yu-Ping Huang. Ultra-efficient frequency conversion in quasi-phase-matched lithium niobate microrings. *Optica*, 6(9):1244–1245, Sep 2019. doi:10.1364/OPTICA.6.001244. URL <http://opg.optica.org/optica/abstract.cfm?URI=optica-6-9-1244>.
- Marcelo Davanco, Jin Liu, Luca Sapienza, Chen-Zhao Zhang, José Vinícius De Miranda Cardoso, Varun Verma, Richard Mirin, Sae Woo Nam, Liu Liu, and Kartik Srinivasan. Heterogeneous integration for on-chip quantum photonic circuits with single quantum dot devices. *Nature Communications*, 8(1):889, Oct 2017. ISSN 2041-1723. doi:10.1038/s41467-017-00987-6. URL <https://doi.org/10.1038/s41467-017-00987-6>.
- C. L. Degen, F. Reinhard, and P. Cappellaro. Quantum sensing. *Rev. Mod. Phys.*, 89:035002, Jul 2017. doi:10.1103/RevModPhys.89.035002. URL <https://link.aps.org/doi/10.1103/RevModPhys.89.035002>.
- Nicolas Gisin, Grégoire Ribordy, Wolfgang Tittel, and Hugo Zbinden. Quantum cryptography. *Rev. Mod. Phys.*, 74:145–195, Mar 2002. doi:10.1103/RevModPhys.74.145. URL <https://link.aps.org/doi/10.1103/RevModPhys.74.145>.
- Xuhan Guo, An He, and Yikai Su. Recent advances of heterogeneously integrated III–v laser on si. *Journal of Semiconductors*, 40(10):101304, oct 2019. doi:10.1088/1674-4926/40/10/101304. URL <https://doi.org/10.1088/1674-4926/40/10/101304>.
- Elizabeth Hemsley, Damien Bonneau, Jason Pelc, Ray Beausoleil, Jeremy L. O’Brien, and Mark G. Thompson. Photon pair generation in hydrogenated amorphous silicon microring resonators. *Scientific Reports*, 6(1):38908, Dec 2016. ISSN 2045-2322. doi:10.1038/srep38908. URL <https://doi.org/10.1038/srep38908>.
- Wei C. Jiang, Xiyuan Lu, Jidong Zhang, Oskar Painter, and Qiang Lin. Silicon-chip source of bright photon pairs. *Opt. Express*, 23(16):20884–20904, Aug 2015. doi:10.1364/OE.23.020884. URL <http://opg.optica.org/oe/abstract.cfm?URI=oe-23-16-20884>.

- Mingwei Jin, Jiayang Chen, Yongmeng Sua, Prajnesh Kumar, and Yuping Huang. Efficient electro-optical modulation on thin-film lithium niobate. *Opt. Lett.*, 46(8):1884–1887, Apr 2021. doi:10.1364/OL.419597. URL <http://opg.optica.org/ol/abstract.cfm?URI=ol-46-8-1884>.
- Shahram Keyvaninia, Gunther Roelkens, Dries Van Thourhout, Christophe Jany, Marco Lamponi, Alban Le Liepvre, Francois Lelarge, Dalila Make, Guang-Hua Duan, Damien Bordel, and Jean-Marc Fedeli. Demonstration of a heterogeneously integrated iii-v/soi single wavelength tunable laser. *Opt. Express*, 21(3):3784–3792, Feb 2013. doi:10.1364/OE.21.003784. URL <http://opg.optica.org/oe/abstract.cfm?URI=oe-21-3-3784>.
- H. J. Kimble. The quantum internet. *Nature*, 453(7198):1023–1030, Jun 2008. ISSN 1476-4687. doi:10.1038/nature07127. URL <https://doi.org/10.1038/nature07127>.
- Michael Kues, Christian Reimer, Piotr Roztock, Luis Romero Cortés, Stefania Sciara, Benjamin Wetz, Yanbing Zhang, Alfonso Cino, Sai T. Chu, Brent E. Little, David J. Moss, Lucia Caspani, José Azaña, and Roberto Morandotti. On-chip generation of high-dimensional entangled quantum states and their coherent control. *Nature*, 546(7660):622–626, Jun 2017. ISSN 1476-4687. doi:10.1038/nature22986. URL <https://doi.org/10.1038/nature22986>.
- J. Lavoie, J. M. Donohue, L. G. Wright, A. Fedrizzi, and K. J. Resch. Spectral compression of single photons. *Nature Photonics*, 7(5):363–366, May 2013. ISSN 1749-4893. doi:10.1038/nphoton.2013.47. URL <https://doi.org/10.1038/nphoton.2013.47>.
- Alan D. Logan, Michael Gould, Emma R. Schmidgall, Karine Hestroffer, Zin Lin, Weiliang Jin, Arka Majumdar, Fariba Hatami, Alejandro W. Rodriguez, and Kai-Mei C. Fu. 400%/w second harmonic conversion efficiency in 14 μm-diameter gallium phosphide-on-oxide resonators. *Opt. Express*, 26(26):33687–33699, Dec 2018. doi:10.1364/OE.26.033687. URL <http://www.osapublishing.org/oe/abstract.cfm?URI=oe-26-26-33687>.
- Xiyuan Lu, Steven Rogers, Thomas Gerrits, Wei C. Jiang, Sae Woo Nam, and Qiang Lin. Heralding single photons from a high-q silicon microdisk. *Optica*, 3(12):1331–1338, Dec 2016. doi:10.1364/OPTICA.3.001331. URL <http://www.osapublishing.org/optica/abstract.cfm?URI=optica-3-12-1331>.
- Xiyuan Lu, Gregory Moille, Anshuman Singh, Qing Li, Daron A. Westly, Ashutosh Rao, Su-Peng Yu, Travis C. Briles, Scott B. Papp, and Kartik Srinivasan. Milliwatt-threshold visible–telecom optical parametric oscillation using silicon nanophotonics. *Optica*, 6(12):1535–1541, Dec 2019. doi:10.1364/OPTICA.6.001535. URL <http://opg.optica.org/optica/abstract.cfm?URI=optica-6-12-1535>.
- Chaoxuan Ma, Xiaoxi Wang, Vikas Anant, Andrew D. Beyer, Matthew D. Shaw, and Shayan Mookherjea. Silicon photonic entangled photon-pair and heralded single photon generation with $\text{car} \geq 12,000$ and $g(2)(0) \leq 0.006$. *Opt. Express*, 25(26):32995–33006, Dec 2017. doi:10.1364/OE.25.032995. URL <http://opg.optica.org/oe/abstract.cfm?URI=oe-25-26-32995>.
- Zhaohui Ma, Jia-Yang Chen, Zhan Li, Chao Tang, Yong Meng Sua, Heng Fan, and Yu-Ping Huang. Ultrabright quantum photon sources on chip. *Phys. Rev. Lett.*, 125:263602, Dec 2020. doi:10.1103/PhysRevLett.125.263602. URL <https://link.aps.org/doi/10.1103/PhysRevLett.125.263602>.
- Neil MacFarlane, Michael R. Kossey, Jasper R. Stroud, Mark A. Foster, and Amy C. Foster. A multi-layer platform for low-loss nonlinear silicon photonics. *APL Photonics*, 4(11):110809, 2019. doi:10.1063/1.5115234. URL <https://doi.org/10.1063/1.5115234>.
- Neil MacFarlane, Mingwei Jin, Zhaohui Ma, Sua Yongmeng, Mark A. Foster, Amy C. Foster, and Yuping Huang. Photon-pair generation in a heterogeneous silicon photonic chip. In *2022 Conference on Lasers and Electro-Optics (CLEO)*, pages 1–2, 2022.
- Delphine Marris-Morini, Vladyslav Vakarin, Joan Manel Ramirez, Qiankun Liu, Andrea Ballabio, Jacopo Frigerio, Miguel Montesinos, Carlos Alonso-Ramos, Xavier Le Roux, Samuel Serna, Daniel Benedikovic, Daniel Chrastina, Laurent Vivien, and Giovanni Isella. Germanium-based integrated photonics from near- to mid-infrared applications. *Nanophotonics*, 7(11):1781–1793, 2018. doi:10.1515/nanoph-2018-0113. URL <https://doi.org/10.1515/nanoph-2018-0113>.
- Jurgen Michel, Jifeng Liu, and Lionel C. Kimerling. High-performance ge-on-si photodetectors. *Nature Photonics*, 4(8):527–534, Aug 2010. ISSN 1749-4893. doi:10.1038/nphoton.2010.157. URL <https://doi.org/10.1038/nphoton.2010.157>.
- Galan Moody, Volker J Sorger, Daniel J Blumenthal, Paul W Juodawlkis, William Loh, Cheryl Sorace-Agaskar, Alex E Jones, Krishna C Balram, Jonathan C F Matthews, Anthony Laing, Marcelo Davanco, Lin Chang, John E Bowers, Niels Quack, Christophe Galland, Igor Aharonovich, Martin A Wolff, Carsten Schuck, Neil Sinclair, Marko Lončar, Tin Komljenovic, David Weld, Shayan Mookherjea, Sonia Buckley, Marina Radulaski, Stephan Reitzenstein, Benjamin Pingault, Bartholomeus Machiels, Debsuvra Mukhopadhyay, Alexey Akimov, Aleksei

- Zheltikov, Girish S Agarwal, Kartik Srinivasan, Juanjuan Lu, Hong X Tang, Wentao Jiang, Timothy P McKenna, Amir H Safavi-Naeini, Stephan Steinhauer, Ali W Elshaari, Val Zwiller, Paul S Davids, Nicholas Martinez, Michael Gehl, John Chiaverini, Karan K Mehta, Jacqueline Romero, Navin B Lingaraju, Andrew M Weiner, Daniel Peace, Robert Cernansky, Mirko Lobino, Eleni Diamanti, Luis Trigo Vidarte, and Ryan M Camacho. 2022 roadmap on integrated quantum photonics. *Journal of Physics: Photonics*, 4(1):012501, jan 2022. doi:10.1088/2515-7647/ac1ef4. URL <https://doi.org/10.1088/2515-7647/ac1ef4>.
- Jeremy L. O’Brien. Optical quantum computing. *Science*, 318(5856):1567–1570, 2007. doi:10.1126/science.1142892. URL <https://www.science.org/doi/abs/10.1126/science.1142892>.
- Jeremy L. O’Brien, Akira Furusawa, and Jelena Vučković. Photonic quantum technologies. *Nature Photonics*, 3(12):687–695, Dec 2009. ISSN 1749-4893. doi:10.1038/nphoton.2009.229. URL <https://doi.org/10.1038/nphoton.2009.229>.
- Swe Z. Oo, Antulio Tarazona, Ali Z. Khokhar, Rafidah Petra, Yohann Franz, Goran Z. Mashanovich, Graham T. Reed, Anna C. Peacock, and Harold M. H. Chong. Hot-wire chemical vapor deposition low-loss hydrogenated amorphous silicon waveguides for silicon photonic devices. *Photon. Res.*, 7(2):193–200, Feb 2019. doi:10.1364/PRJ.7.000193. URL <http://www.osapublishing.org/prj/abstract.cfm?URI=prj-7-2-193>.
- Peter Schnauber, Anshuman Singh, Johannes Schall, Suk In Park, Jin Dong Song, Sven Rodt, Kartik Srinivasan, Stephan Reitzenstein, and Marcelo Davanco. Indistinguishable photons from deterministically integrated single quantum dots in heterogeneous gaas/si₃n₄ quantum photonic circuits. *Nano Letters*, 19(10):7164–7172, Oct 2019. ISSN 1530-6984. doi:10.1021/acs.nanolett.9b02758. URL <https://doi.org/10.1021/acs.nanolett.9b02758>.
- Neil Sinclair, Erhan Saglamyurek, Hassan Mallahzadeh, Joshua A. Slater, Mathew George, Raimund Ricken, Morgan P. Hedges, Daniel Oblak, Christoph Simon, Wolfgang Sohler, and Wolfgang Tittel. Spectral multiplexing for scalable quantum photonics using an atomic frequency comb quantum memory and feed-forward control. *Phys. Rev. Lett.*, 113:053603, Jul 2014. doi:10.1103/PhysRevLett.113.053603. URL <https://link.aps.org/doi/10.1103/PhysRevLett.113.053603>.
- Trevor J. Steiner, Joshua E. Castro, Lin Chang, Quynh Dang, Weiqiang Xie, Justin Norman, John E. Bowers, and Galan Moody. Ultrabright entangled-photon-pair generation from an AlGaAs-on-insulator microring resonator. *PRX Quantum*, 2:010337, Mar 2021. doi:10.1103/PRXQuantum.2.010337. URL <https://link.aps.org/doi/10.1103/PRXQuantum.2.010337>.
- Cheng Wang, Mian Zhang, Xi Chen, Maxime Bertrand, Amirhassan Shams-Ansari, Sethumadhavan Chandrasekhar, Peter Winzer, and Marko Lončar. Integrated lithium niobate electro-optic modulators operating at cmos-compatible voltages. *Nature*, 562(7725):101–104, Oct 2018. ISSN 1476-4687. doi:10.1038/s41586-018-0551-y. URL <https://doi.org/10.1038/s41586-018-0551-y>.
- Ke-Yao Wang and Amy C. Foster. Ultralow power continuous-wave frequency conversion in hydrogenated amorphous silicon waveguides. *Opt. Lett.*, 37(8):1331–1333, Apr 2012. doi:10.1364/OL.37.001331. URL <http://www.osapublishing.org/ol/abstract.cfm?URI=ol-37-8-1331>.
- Ke-Yao Wang, Vesselin G. Velez, Kim Fook Lee, Abijith S. Kowligy, Prem Kumar, Mark A. Foster, Amy C. Foster, and Yu-Ping Huang. Multichannel photon-pair generation using hydrogenated amorphous silicon waveguides. *Opt. Lett.*, 39(4):914–917, Feb 2014. doi:10.1364/OL.39.000914. URL <http://www.osapublishing.org/ol/abstract.cfm?URI=ol-39-4-914>.
- Xiang Zhang, Yanbing Zhang, Chunle Xiong, and Benjamin J Eggleton. Correlated photon pair generation in low-loss double-stripe silicon nitride waveguides. *Journal of Optics*, 18(7):074016, jun 2016. doi:10.1088/2040-8978/18/7/074016. URL <https://doi.org/10.1088/2040-8978/18/7/074016>.